A Journal of the Gesellschaft Deutscher Chemiker

Angewandte International Edition GDCh Chemie

www.angewandte.org

Accepted Article

Title: Solid Electrolyte Interphase Design for Aqueous Zn Batteries

Authors: Dan Li, Longsheng Cao, Tao Deng, Sufu Liu, and Chunsheng Wang

To be cited as: *Angew. Chem. Int. Ed.* 10.1002/anie.202103390

Link to VoR: https://doi.org/10.1002/anie.202103390

WILEY-VCH

10.1002/anie.202103390

WILEY-VCH

RESEARCH ARTICLE

Solid Electrolyte Interphase Design for Aqueous Zn Batteries

Dan Li,[a, †] Longsheng Cao,[a, †] Tao Deng,[a] Sufu Liu,[a] and Chunsheng Wang*[a, b]

[a] Dr. D. Li, Dr. L. Cao, Dr. T. Deng, Dr. S. Liu, Prof. C. Wang
Department of Chemical and Biomolecular Engineering, University of Maryland, College Park, MD 20742, United States
E-mail: cswang@umd.edu
[b] Prof. C. Wang
Department of Chemistry and Biochemistry, University of Maryland, College Park, MD 20742, United States
[†] These authors contributed equally to this work.

Supporting information for this article is given via a link at the end of the document.

Abstract: Aqueous Zn batteries are challenged by water decomposition and dendrite growth due to the absence of a dense Zn-ion conductive solid electrolyte interphase (SEI) to inhibit hydrogen evolution reaction (HER). Here, we design a low-concentration aqueous $Zn(OTF)_2$-$Zn(NO_3)_2$ electrolyte to in situ form a robust inorganic ZnF_2-$Zn_5(CO_3)_2(OH)_6$-organic bi-layer SEI where the inorganic inner layer promotes Zn-ion diffusion while the organic outer layer suppresses water penetration. Comprehensive characterization reveals that insulating $Zn_5(OH)_8(NO_3)_2{\cdot}2H_2O$ layer is first formed on Zn anode surface by self-terminated chemical reaction of NO_3^- with Zn^{2+} and OH^- generated via HER, and then it transforms into Zn-ion conducting $Zn_5(CO_3)_2(OH)_6$ which in-turn promotes ZnF_2 formation as the inner layer. The organic dominated outer layer is formed by the reduction of OTF^-. The in situ formed SEI enables a high Coulombic efficiency (CE) of 99.8% for 200 h in Ti||Zn cells, and a high energy density (168 Wh kg^{-1}) with 96.5% retention for 700 cycles in Zn||MnO_2 cells with a low Zn/MnO_2 capacity ratio of 2:1.

Introduction

Aqueous Zn battery is promising for large-scale energy storage owing to its high theoretical capacity (820 mAh g^{-1}), high abundance of Zn, and intrinsic safety[1]. Since the reduction potential of Zn (−0.762 V vs standard hydrogen electrode (SHE)) is negative than that of hydrogen evolution reaction (HER), water is reduced to H_2 during Zn deposition (**Fig. 1a**), which changes the local pH to a strong alkaline[2]. The alkaline environment corrodes Zn anode surface by formation of porous $Zn(OH)_2$ and ZnO[3]. The inhomogeneous morphology of the $Zn(OH)_2$ and ZnO-based layer on Zn anode surface induces the Zn dendrite growth, reducing the Coulombic efficiency (CE) of Zn plating/stripping and leading to rapid battery failure[4].

To suppress water decomposition and Zn dendrite growth, extensive efforts are devoted to constructing artificial solid electrolyte interphase (SEI) by coating inorganic[5] or polymer[6] on Zn surface that allow Zn^{2+} to transport but block water penetration to Zn surface. Unfortunately, these interphases suffer from crack and/or degradation during repeat volume changes of cycles[7]. Since these artificial SEI are not self-repairable as that of in-situ formed SEI, they gradually lose the function of protection. Therefore, it is highly desired to form SEI by in-situ decomposition of electrolyte components on electrode surface. The decomposition of organic triflate anion (OTF^-)[8] in high-concentration aqueous 21 m LiTFSI+7 m LiOTF electrolyte has been proved to form electrically insulating and ionically conductive fluorinated inorganic-organic composite SEI, effectively protecting anode and preventing electrolyte decomposition while allowing lithium ion to cross in lithium batteries. However, the in-situ formation of robust fluorinated SEI in low-concentration aqueous Zn batteries has been challenged. Even if a SEI can be formed during Zn plating in a low-concentration aqueous electrolyte, the hydrogen gas evolution during SEI formation will blow the formed SEI away. To promote SEI formation while suppressing H_2 gas generation during Zn plating in low-concentration aqueous electrolytes, additives with a high reduction potential are normally added. However, long Zn plating/stripping cycles are needed for forming a dense SEI since H_2 gas evolution cannot be completely inhibited by additives, which reduces the average CE.

Here, we prevented the H_2 gas evolution during Zn plating/stripping by adding 20 mM $Zn(NO_3)_2$ additive into aqueous 3 M $Zn(OTF)_2$ electrolyte (denoted as $Zn(OTF)_2$-$Zn(NO_3)_2$) to chemically form a thin and dense $Zn_5(OH)_8(NO_3)_2{\cdot}2H_2O$ passivation layer upon the contact of Zn with electrolyte which blocks water penetration. Since the passivation layer is self-repairable, hydrogen evolution will be prevented even if the passivation layer cracks during Zn plating/stripping cycles. Upon contact of Zn with $Zn(OTF)_2$-$Zn(NO_3)_2$ electrolyte, water reduces on Zn surface generating a local alkaline environment, which triggers the thermodynamically and kinetically favourable reaction between Zn and NO_3^-/OH^- and forms an electrically and ionically resistive $Zn_5(OH)_8(NO_3)_2{\cdot}2H_2O$ passivation layer[9] before Zn electrodeposition. The $Zn_5(OH)_8(NO_3)_2{\cdot}2H_2O$ layer inhibits water penetration onto Zn surface, which allows reduction of OTF^- anion to form SEI on Zn surface. As an intermediate template layer, $Zn_5(OH)_8(NO_3)_2{\cdot}2H_2O$ layer gradually transforms into a more stable Zn-ion conductive $Zn_5(CO_3)_2(OH)_6$ layer through metathesis reaction due to the lower solubility product (2.0×10^{-15}) of $Zn_5(CO_3)_2(OH)_6$ than that (7.4×10^{-11}) of $Zn_5(OH)_8(NO_3)_2{\cdot}2H_2O$[9], when CO_3^{2-} forms from the reduction of $Zn(OTF)_2$. At the same time, the organic components out-layer forms from the reaction between $(CF_3SO_3)^-$ and NO_3^- acting as flexible protection layer, and the zinc ion conducting ZnF_2 forms in the inner part (**Fig. 1b**). The highly flexible organic outer layer prevents SEI from crack due to volumetric change and facilitates solvated Zn ion to immigrate. The hydrophobic ZnF_2 in the inner layer further removes solvated water, and suppresses water decomposition and Zn dendrite growth by preventing direct contact of zinc with water but allows Zn^{2+} to transport through. This robust SEI enhanced the Zn plating/stripping CE to 99.8% in 200 h. The Zn||MnO_2 batteries show a high capacity stability with an extremely low capacity delay rate of only 0.005% per cycle for 700 cycles.

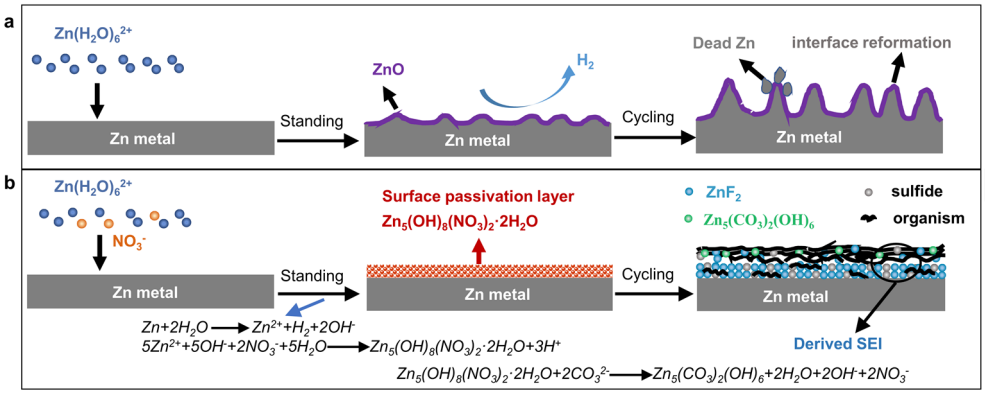

Fig. 1 Illustration of surface evolution mechanism. a) Zn dendrite growth in aqueous electrolytes. Water passivation induced porous ZnO layer (purple) constantly breaks and re-forms, leading to non-uniform Zn electrodeposition, dendrite, and dead Zn during Zn plating/stripping. b) ZnF_2-$Zn_5(CO_3)_2(OH)_6$-organic SEI formation mechanism. The presence of NO_3^- promotes the formation of electrically and ionically insulating $Zn_5(OH)_8(NO_3)_2{\cdot}2H_2O$ layer (red), which subsequently transforms into an electrically insulating but ionically conductive SEI with ZnF_2-$Zn_5(CO_3)_2(OH)_6$ inner part coated by the organic outer part.

Results and Discussion

In situ formation of SEI on Zn anodes

The Zn surface passivation was formed by immersing Zn plate in $Zn(OTF)_2$-$Zn(NO_3)_2$ electrolyte (pH=3.8). After 4 h treatment in $Zn(OTF)_2$-$Zn(NO_3)_2$ electrolyte at room temperature, the color of Zn metal surface changed from light silver to gray (**Supplementary Fig. 1**). X-ray powder diffraction (XRD) in **Supplementary Fig. 2** demonstrated that $Zn_5(OH)_8(NO_3)_2{\cdot}2H_2O$ passivation layer was formed based on the chemical reaction[9] in **Fig. 1b**. For comparsion, Zn was also immersed in $Zn(OTF)_2$ reference aqueous electrolyte (pH=3.6). However, well-identified peaks of $ZnO/Zn(OH)_2$ (**Supplementary Fig. 3**) were observed. The Zn surface passivation layer morphologies were characterized using the scanning electron microscopy (SEM). **Supplementary Fig. 4** showed that $Zn_5(OH)_8(NO_3)_2{\cdot}2H_2O$ passivation layer presented a compact sheet stacking morphology, which can suppress water decomposition by separating water from Zn anode, confirmed by a smaller change of pH values (from 3.8 to 4.0 than that from 3.6 to 4.0 in $Zn(OTF)_2$ electrolyte) during Zn immersion test. However, the Zn plate surface after treatment in $Zn(OTF)_2$ electrolyte showed cracked surface. The electrochemical behaviors of Zn electrode in different electrolytes were investigated using Zn||Ti cells with cyclic voltammetry (CV). As shown in the CV curves in $Zn(OTF)_2$-$Zn(NO_3)_2$ electrolyte (**Fig. 2a**), in the first cathodic scan, the in-situ formed $Zn_5(OH)_8(NO_3)_2{\cdot}2H_2O$ passivation layer suppressed Zn plating potential to a very low potential of -0.37 V, with a small Zn stripping peak at a very high potential of 0.31 V. The Zn plating/stripping overpotentials gradually reduced with charge/discharge cycles and showed a normal Zn plating peak at -0.15 V and Zn stripping peak at +0.15 V at the 10th charge/discharg cycle. Therefore, the $Zn_5(OH)_8(NO_3)_2{\cdot}2H_2O$ layer gradually became a Zn-ion conductor during Zn plating/stripping cycles. In contrst, Zn plating/stripping peaks at +0.15/-0.15 V were observed in the $Zn(OTF)_2$ reference electrolyte (**Supplementary Fig. 5**) due to formation of porous $ZnO/Zn(OH)_2$ layer on Zn.

The formation of $Zn_5(OH)_8(NO_3)_2{\cdot}2H_2O$ passivation layer is attributed to the unique Zn^{2+} solvation sheath structure in bulk electrolyte. Nuclear Magnetic Resonance (NMR) demonstrated that only 20 mM NO_3^- additive can move the ^{65}Zn chemical shift from 2.0 ppm in $Zn(OTF)_2$ reference electrolyte to 0.7 ppm in $Zn(OTF)_2$-$Zn(NO_3)_2$ electrolyte (**Supplementary Fig. 6a**), indicating a shielding effect of the solvation sheath on Zn nucleus. This is because that NO_3^- is involved in solvation sheath and replaces some OTF^- due to larger electron-donating ability of NO_3^- than that of OTF^-. Additionally, the ^{17}O chemical shift of OTF^- showed a downshift with the addition of NO_3^- (**Supplementary Fig. 6b**), confirming that NO_3^- anions entered the Zn^{2+} solvation sheath. Both ^{65}Zn and ^{17}O NMR spectroscopy demonstrated that Zn^{2+} preferentially coordinates with NO_3^- instead of OTF^-, which is beneficial for the generation of $Zn_5(OH)_8(NO_3)_2{\cdot}2H_2O$.

During 10 activation cycles, insulating $Zn_5(OH)_8(NO_3)_2{\cdot}2H_2O$ layer gradually converts into Zn-ion conducting $Zn_5(CO_3)_2(OH)_6$ SEI as evidenced by XRD (**Supplementary Fig. 2**), which enables reversible Zn plating/stripping (**Fig. 2a**), but suppresses water reduction. The conversion of $Zn_5(OH)_8(NO_3)_2{\cdot}2H_2O$ into $Zn_5(CO_3)_2(OH)_6$ is attributed to the replacement of NO_3^- by CO_3^-, which are generated mainly from OTF^- reduction with minor contribution from dissolved CO_2, because the solubility product (2.0×10^{-15}) of $Zn_5(CO_3)_2(OH)_6$ in water is three order of magnitude lower than that (7.4×10^{-11}) of $Zn_5(OH)_8(NO_3)_2{\cdot}2H_2O$[9]. To validate the conversion of $Zn_5(OH)_8(NO_3)_2{\cdot}2H_2O$ into $Zn_5(CO_3)_2(OH)_6$ through reduction of OTF^- into CO_3^-, synthesized $Zn_5(OH)_8(NO_3)_2{\cdot}2H_2O$[10] powers were coated on inert Ti electrode and scanned using CV in an inert electrolyte, i.e. 1M NaCl aqueous electrolyte (**Supplementary Fig. 7a-d**). Since the insulative $Zn_5(OH)_8(NO_3)_2{\cdot}2H_2O$ cannot transite into Zn-ion conductive $Zn_5(CO_3)_2(OH)_6$ in 1M NaCl aqueous electrolyte, the Zn-ion insulating $Zn_5(OH)_8(NO_3)_2{\cdot}2H_2O$ layer on Ti shifted the Zn plating and water reduction potential to -0.6 V vs Zn/Zn^{2+}, while the Zn can be normally stripped at a low potential of 0.15 V due to formation of micro-cracks (**Supplementary Fig. 7d**). However, after 10 cycles, the Zn plating/stripping was completely inhibited on $Zn_5(OH)_8(NO_3)_2{\cdot}2H_2O$ coated on Ti electrode because the formation of ZnO during charge/discharge sealed the cracks (**Supplementary Fig. 7d**). Therefore, the formation of insulating $Zn_5(OH)_8(NO_3)_2{\cdot}2H_2O$ passivation layer on Zn after immersion in $Zn(OTF)_2$-$Zn(NO_3)_2$ electrolyte suppressed water decomposition while the OTF^- reduction during followed activation cycles converted the insulating $Zn_5(OH)_8(NO_3)_2{\cdot}2H_2O$ layer into Zn-ion conducting $Zn_5(CO_3)_2(OH)_6$ SEI without damaging from H_2 evolution.

10.1002/anie.202103390

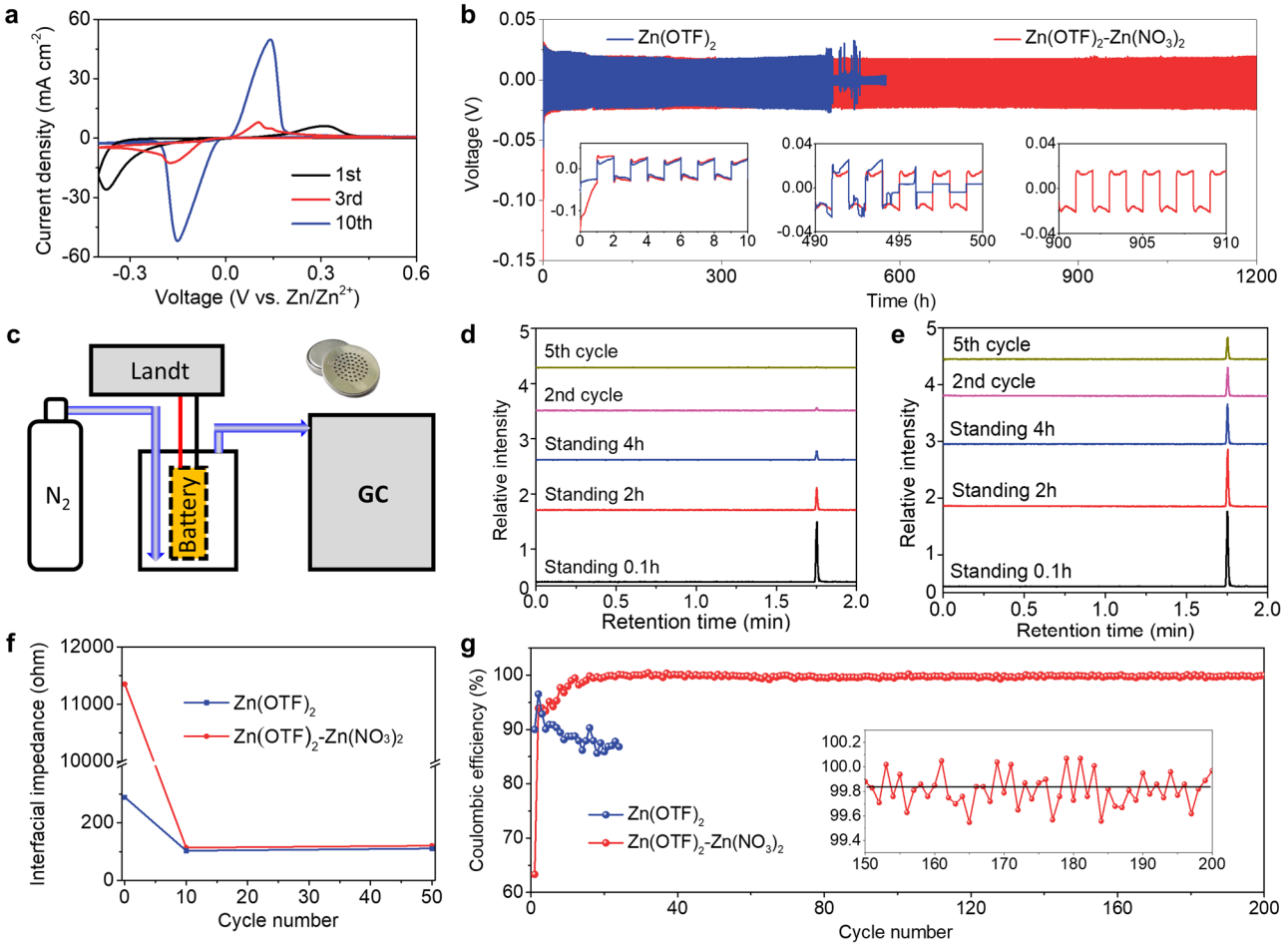

Fig. 2 a) CV curves of Zn||Ti cells with $Zn(OTF)_2$-$Zn(NO_3)_2$ electrolyte. b) Galvanostatic Zn plating/stripping in the Zn||Zn symmetrical cells at 0.5 mA cm^{-2} and 0.5 mAh cm^{-2}. c) Schematic illustration of the home-built system for in situ detection of hydrogen gas evolution using gas chromatograph (GC). Peak of hydrogen gas released from Zn||Zn cells using d) $Zn(OTF)_2$-$Zn(NO_3)_2$ and e) $Zn(OTF)_2$ electrolytes before and after cycling. f) Interfacial impedance measured from Zn||Zn cells in $Zn(OTF)_2$-$Zn(NO_3)_2$ and $Zn(OTF)_2$ electrolytes during cycling. g) Zn plating/stripping CE in different electrolytes (inset: Magnified view of Zn plating/stripping CE in $Zn(OTF)_2$-$Zn(NO_3)_2$ electrolyte).

The effect of $Zn(NO_3)_2$ additive on the reversibility of Zn plating/stripping in $Zn(OTF)_2$ electrolyte was investigated using a Zn||Zn symmetric cell under galvanostatic condition (**Fig. 2b**). After the initial activation, the symmetric Zn||Zn cell using $Zn(OTF)_2$-$Zn(NO_3)_2$ electrolyte exhibited steady charge/discharge process over 1200 h. In contrast, the Zn||Zn cell using $Zn(OTF)_2$ reference electrolyte shorted after 480 h. The larger average overpotential (~77 mV) of Zn||Zn cells at 0.5 mA cm^{-2} in the first cycle in $Zn(OTF)_2$-$Zn(NO_3)_2$ electrolyte than that (~30 mV) in $Zn(OTF)_2$ electrolyte (**Fig. 2b**) is attributed to the large Zn^{2+} transport resistance in the $Zn_5(OH)_8(NO_3)_2{\cdot}2H_2O$ passivation layer than that in porpous ZnO/$Zn(OH)_2$ layer. However, the overpotential of Zn plating/stripping in $Zn(OTF)_2$-$Zn(NO_3)_2$ electrolyte gradually decreased and eventually stabilized at ~20 mV due to the transformation of ionic-resistant $Zn_5(OH)_8(NO_3)_2{\cdot}2H_2O$ passivation layer into a high Zn^{2+} transport SEI. Furthermore, the plating/stripping reversibility of Zn anode in two electrolytes were compared at a high current density of 10 mA cm^{-2} and a high capacity of 10 mAh cm^{-2}. As shown in **Supplementary Fig. 8**, the cell using $Zn(OTF)_2$ electrolyte shorted after only 29 h, while the cell using $Zn(OTF)_2$-$Zn(NO_3)_2$ electrolyte operated steadily for >90 h, confirming the robustness of SEI even at a high current density and high area capacity. The chemical formation of water-proof passivation layer on Zn anodes, followed by gradual convertion into zinc-ion conductive SEI during Zn plating/stripping cycles, lays the foundation for designing high power, high energy and long cycle Zn batteries.

The chemically pre-formed $Zn_5(OH)_8(NO_3)_2{\cdot}2H_2O$ passivation layer promoted the formation of $Zn_5(CO_3)_2(OH)_6$ SEI by supressing H_2 evolution. The hydrogen gas evolution during Zn plating/stripping in two electrolytes was investigated by operando monitoring evolved hydrogen using a home-built system (**Fig. 2c**). The evolved hydrogen gas, released from meshed Zn||Zn cells, was transferred from a sealed container to an online gas chromatograph (GC) using nitrogen as a carrier gas. The low and also rapidly reduced hydrogen evolution in $Zn(NO_3)_2$-contained electrolyte (**Fig. 2d**) during Zn palting/stripping cycles, contrary to the reference electrolyte (**Fig. 2e**), confirmed the effective suppression of hydrogen evolution by pre-formed passivation layer.

The Zn-ion conduction increase during transition from $Zn_5(OH)_8(NO_3)_2{\cdot}2H_2O$ to $Zn_5(CO_3)_2(OH)_6$ was confirmed by interfacial impedance spectroscopy (EIS). The EIS of Zn||Zn symmetric cells after charge/discharge at 0.5 mA cm^{-2} and 0.5

mAh cm^{-2} was recorded. In **Fig. 2f** and **Supplementary Fig. 9**, the interface impedance (impedance of charge-transfer plus passivation interphase resistance) of Zn||Zn cells in $Zn(OTF)_2$-$Zn(NO_3)_2$ electrolyte before cycle show ionic insulating nature with a large interface impedance of 11350 ohm due to the formation of $Zn_5(OH)_8(NO_3)_2{\cdot}2H_2O$ passivation layer. However, the interface impedance quickly reduced to 114 ohm after 10 plating/stripping cycles because Zn plating/stripping triggered the transformation of ionic-insulating $Zn_5(OH)_8(NO_3)_2{\cdot}2H_2O$ layer into a fast-ion conducting $Zn_5(CO_3)_2(OH)_6$ layer. After 10 Zn plating/stripping cycles, the interface resistance of dense $Zn_5(CO_3)_2(OH)_6$ (**Supplementary Fig. 4c-e)** passivated Zn is slightly larger than that of passivated by porous undesirable byproducts (such as $Zn(OH)_2$, $xZnCO_3{\cdot}yZn(OH)_2{\cdot}zH_2O$ and ZnO) formed on Zn surface with hydrogen evolution interference in $Zn(OTF)_2$ electrolyte (**Supplementary Fig. 3, Supplementary Fig. 4f-h**). Different from phase-transition induced resistance-reduction of Zn||Zn cell in the initial 10 charge/discharge cycles in $Zn(OTF)_2$-$Zn(NO_3)_2$ electrolyte, the initial decrease in the interface resistance for Zn||Zn cell in $Zn(OTF)_2$ electrolyte is mainly attributed to activation process. Therefore, the presence of $Zn_5(OH)_8(NO_3)_2{\cdot}2H_2O$ passivation layer inhibited Zn corrosion and created a water/gas-free micro-environment on Zn surface, promoting the formation of a robust SEI.

The impact of NO_3^- additive on Zn plating/stripping CE was investigated using Zn||Ti cells at 1 mA cm^{-2} and 0.5 mAh cm^{-2} (**Fig. 2g, Supplementary Fig. 10**). **Fig. 2g** showed that the CE in $Zn(OTF)_2$-$Zn(NO_3)_2$ electrolyte quickly increased from 63.3% at the first cycle to 99.8% within the initial 20 cycles with an average CE of 95.7%, and then stabilized at >99.8% for >200 cycles, with an average CE of 99.4% for the entire 200 cycles. In contrast, the CE in the $Zn(OTF)_2$ reference electrolyte reached ~95% in the initial few cycles, but quickly drop to <90% after 10 cycles before short circuit at the 25th cycle. Therefore, the NO_3^- additive effectively suppressed side reactions between Zn and water, increasing Zn plating/stripping CE. The activation process along with phase transition from $Zn_5(OH)_8(NO_3)_2{\cdot}2H_2O$ into $Zn_5(CO_3)_2(OH)_6$ based SEI in $Zn(OTF)_2$-$Zn(NO_3)_2$ electrolyte was also evidenced by quickly reduced overpotential from 205 mV at the beginning to 85 mV at 200th cycle (**Supplementary Fig. 11a**, **b).** Although the Zn plating/stripping behavior of Zn||Ti cells in $Zn(OTF)_2$ electrolyte shows a low overpotential (71 mV to 40 mV) due to low diffusion resistance of porous passivation layer, the Zn stripping curves are not stable due to Zn dendrite growth (**Supplementary Fig. 11c**, **d)**.

Morphology and structure of SEI on Zn anodes

The Zn deposition morphologies and cross-sectional views of Zn-metal anode in different electrolytes were observed using SEM (**Fig. 3**). Zn surface after 100 cycles in $Zn(OTF)_2$ reference electrolyte showed mossy growth (**Fig. 3a, b**), where a cross-section of the 20 μm thick plated Zn reveals highly porous Zn deposition (**Fig. 3c**). This morphology was caused by continuous side reactions between Zn and electrolyte, as evidenced by a low CE (< 90%) (**Fig. 2d**) and poor cycling stability. In contrast, in $Zn(OTF)_2$-$Zn(NO_3)_2$ electrolyte, the Zn metal maintained a dense and smooth surface (**Fig. 3d, e**), evidenced by decreased thickness of cycled Zn from 20 μm in $Zn(OTF)_2$ reference electrolyte to 9.5 μm (**Fig. 3c, f**). Therefore, NO_3^- induced hydrophobic SEI on Zn surface (**Supplementary Fig. 12**) effectively suppressed Zn dendrite growth and parasitic reactions between Zn anode and water, leading to compact and smooth Zn deposition. Furthermore, the surface passivation layer in different electrolytes were investigated using transmission electron microscopy (TEM) (**Supplementary Fig. 13**). A 3.5 nm SEI layer was observed on the surface of cycled Zn in $Zn(OTF)_2$-$Zn(NO_3)_2$ electrolyte, confirming the NO_3^- induced formation of SEI layer.

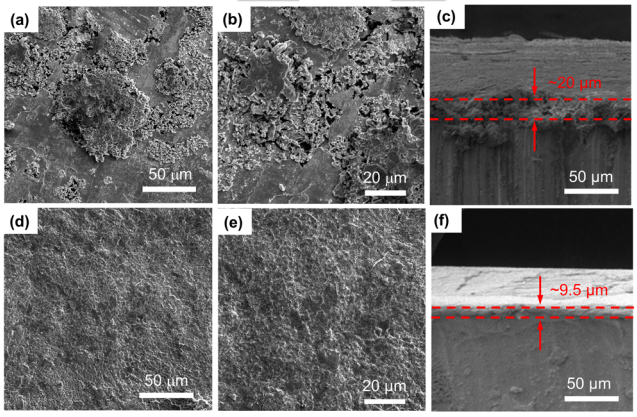

Fig. 3 SEM images of surface and cross-section Zn electrodes recovered from Zn||Zn symmetrical cells after 100 plating/striping cycles in (a–c) $Zn(OTF)_2$, and (d–f) $Zn(OTF)_2$-$Zn(NO_3)_2$ electrolytes. (a, b) and (d, e) are surface morphologies of Zn metal. Red lines in SEM images (c, f) indicated the etching depth of the Zn metal cycled in different electrolytes.

The SEI composition on the Zn anode after 50 plating/stripping cycles was analyzed using X-ray photoelectron spectroscopy (XPS) facilitated by Ar^+ sputtering. On the surface (before sputtering) of SEI in $Zn(OTF)_2$-$Zn(NO_3)_2$ electrolyte, N exists as organic N-C at ~400 eV[11], rather than inorganic NO_3^-, from the N 1s spectrum (**Fig. 4a)**, because $Zn_5(OH)_8(NO_3)_2{\cdot}2H_2O$ converts into $Zn_5(CO_3)_2(OH)_6$, consistent with XRD results (**Supplementary Fig. 2**). In addition, organic components (CF_3, C-O, C-S, C-N; 90.3%) with minor inorganic CO_3^{2-} species (9.7%) were also detected on the SEI surface, as evdiced by the C 1s spectra in **Fig. 4b**. The C-N and C-O species arise from reaction products of NO_3^- and OTF^-. The CF_3 and C-S species arise from either of incomplete reduction products of OTF^- or trace $Zn(OTF)_2$ residue on Zn surface. The decomposition of OTF^- was further verified by ZnS and $ZnSO_3$ signals in S 2p spectrum (**Supplementary Fig. 14**). The inorganic CO_3^{2-} species, formed from either of decomposition of $Zn(OTF)_2$ or dissolved CO_2 in electrolytes, participated in the formation of $Zn_5(CO_3)_2(OH)_6$. The SEI surface also contains organic CF_3 (94.7%) with minor inorganic ZnF_2 (5.3%) (F 1s spectrum in **Fig. 4c)**. The organic fluorine species arises from either of incomplete reduction products of $Zn(OTF)_2$ or trace $Zn(OTF)_2$ residue on Zn surface, while inorganic ZnF_2 is due to $Zn(OTF)_2$ reduction. Therefore, the topmost surface is mainly composed of organic components, including C-N and CF_3.

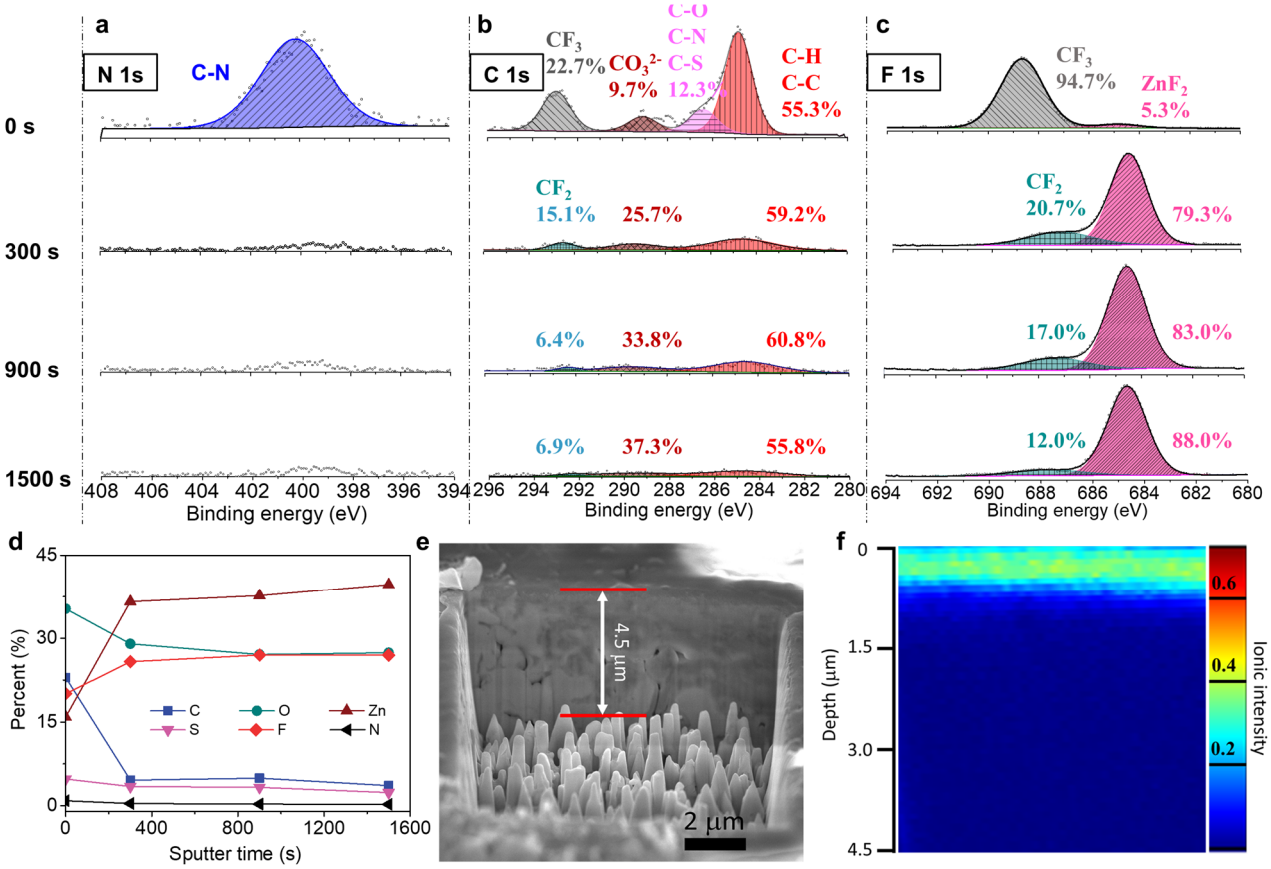

Fig. 4 The composition of the SEI layer. X-ray photoelectron spectroscopy (XPS) of a) N 1s, b) C 1s, and c) F 1s, which are displayed in rows, with corresponding durations of Ar^+ sputtering in columns. d) Atomic composition of the SEI on Zn after 50 plating/stripping cycles in $Zn(OTF)_2$-$Zn(NO_3)_2$ electrolyte. (e, f) The time-of-flight secondary-ion mass spectrometry (TOF-SIMS) analysis of the SEI using a Ga^+ ion beam of 5 μm × 5 μm area. e) The crater sputtered by the Ga^+ ion beam. f) TOF-SIMS analysis for the F element.

After 300 s sputtering, the organic N-C peak disappeared (**Fig. 4a**), in consistent with C 1s spectrum (**Fig. 4b**). Upon further sputtering to 1500 s, no organic N-C peak was detected. However, the content of inorganic CO_3^{2-} species increased, while that of CF_2, from the reduction of $Zn(OTF)_2$ decreased (C element in **Fig. 4b**), although the signal intensity of C element obviously decreased compared with that before sputtering. As for F element, the content of inorganic ZnF_2 increased from 79.3% at 300 s sputtering to 88.0% at 1500 s sputtering, while that of organic CF_2 peak decreased from 20.7% at 300 s sputtering to 12.0% at 1500 s sputtering (**Fig. 4c**). Therefore, the SEI contacting with Zn is composed of ZnF_2 dominated inorganic components.

Fig. 4d summarized the element distribution across the SEI recovered from $Zn(OTF)_2$-$Zn(NO_3)_2$ electrolyte. From the SEI surface to the interface at SEI/Zn, the organic components gradualy decreased, while the inorganic components increased, and ZnF is rich in SEI at the SEI/Zn interface, confirming that the SEI consist of an organic-rich outer layer and inorganic ZnF_2-rich inner layer.

In summary, trace amount of NO_3^- additive promotes decomposition of $Zn(OTF)_2$ salt and stabilizes the deposition product on the Zn surface in low-concentration aqueous electrolyte, facilitating the generation of a dense SEI where ZnF_2-$Zn_5(CO_3)_2(OH)_6$ inner part was coated by organic species outer part. Besides, F element distribution of the SEI was further investigated using time-of-flight secondary-ion mass spectrometry (TOF-SIMS) at various sputtering depths. The void-free crater in **Fig. 4e** revealed dense Zn plating, while a large amount of F element exists within the surface layer (**Fig. 4f**), implying the uniformity of the SEI. In contrast, no decomposed component, like ZnF_2, ZnS, or $ZnSO_3$, was found on a Zn electrode recovered from the $Zn(OTF)_2$ reference electrolyte (**Supplementary Fig. 15**).

Electrochemical performance of Zn-metal full cells

The $Zn(OTF)_2$-$Zn(NO_3)_2$ aqueous electrolyte enabled Zn||MnO_2 full cells to achieve high energy density and long cycle life. Tunnel-structured β-MnO_2 with a high theoretical capacity of 308 mAh/g (0.5 Zn per MnO_2) was used as a cathode. First, the electrochemical performance of MnO_2 cathode in two electrolytes was investigated using CV at 0.1 mV/s in Zn||MnO_2 cells with a high Zn-to-MnO_2 capacity ratio (N/P) of 3.0 to reflect MnO_2 behavior. MnO_2 in both electrolytes featured two redox peaks (**Fig. 5a**), consistent with the previous work[12]. The polarization voltage of the cell with NO_3^- additive is slightly larger than that without NO_3^- additive, which is apparently associated with the dense SEI-induced overpotential. Charge-discharge curves at various C-rates in $Zn(OTF)_2$-$Zn(NO_3)_2$ electrolyte are presented in **Fig. 5b**. When the rate was set as 0.5 C, the cell showed a reversible capacity of 268.1 mAh g^{-1} (168 Wh kg^{-1} based on the cathode and anode). At high current density of 5 C and 10 C, Zn||MnO_2 cells

with $Zn(OTF)_2$-$Zn(NO_3)_2$ electrolyte showed high capacity retention of 58.0% and 49.3% of that at 0.5 C, respectively. This indicated a strong tolerance to the rapid Zn^{2+} ions insertion/extraction for MnO_2 cathode and transfer kinetics through fluorinated SEI for Zn anode. In addition, the cell using $Zn(OTF)_2$ reference electrolyte showed similar rate performance, verifying the fast kinetics of aqueous electrolyte (**Supplementary Fig. 16**).

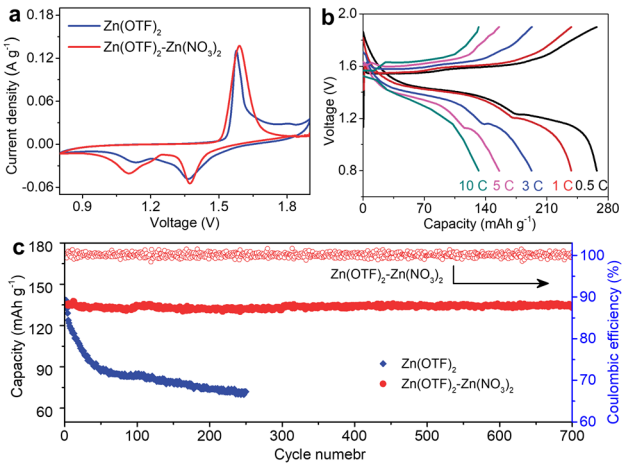

Fig. 5 Electrochemical performance of $Zn||MnO_2$ cells using $Zn(OTF)_2$-$Zn(NO_3)_2$ and $Zn(OTF)_2$ electrolytes. a) CV of $Zn||MnO_2$ full cells at a scan rate of 0.1 mV/s. b) Charge-discharge profiles at various current density in $Zn(OTF)_2$-$Zn(NO_3)_2$ electrolytes. c) Long-term cycling performance of the $Zn||MnO_2$ cells in $Zn(OTF)_2$-$Zn(NO_3)_2$ and $Zn(OTF)_2$ electrolytes with 0.1 M Mn^{2+} to suppress Mn^{2+} dissolution at 10 C.

The high Zn plating/stripping efficiency and long cycle life of MnO_2 cathode enable a high energy $Zn||MnO_2$ full cell with a low N/P (2.0). The cyclic stability of $Zn||MnO_2$ cells using $Zn(OTF)_2$-$Zn(NO_3)_2$ electrolyte outperformed their counterparts with $Zn(OTF)_2$ electrolyte at a charge/discharge rate of 10 C (**Fig. 5c**). The cell with $Zn(OTF)_2$-$Zn(NO_3)_2$ electrolyte exhibit a 96.5% capacity retention after 700 cycles, whereas the cell with $Zn(OTF)_2$ electrolyte only maintained <60% capacity (from 138.2 to 72.0 mAh g^{-1}) after 250 cycles at 10 C, indicating enhanced reversibility of Zn anode protected by NO_3^- additive induced SEI even during rapid plating/stripping at a high current density.

Conclusion

We introduced NO_3^- additive into low-concentration aqueous $Zn(OTF)_2$ electrolyte to chemically form insulating passivation layer, suppressing water decomposition. Then, the insulating passivation layer converted into Zn-ion conductive SEI during initial Zn plating/stripping activation cycles with inhibited hydrogen gas interference. NO_3^- additive plays two key roles in promoting SEI formation and electrochemical stability over long-term operation: (1) Upon contact with Zn anode in aqueous electrolyte, NO_3^- forms electrically and ionically insulating $Zn_5(OH)_8(NO_3)_2{\cdot}2H_2O$ passivation layer, effectively creating water-free environment on Zn surface and avoiding the flow away of SEI components; (2) During Zn plating/stripping, solvated NO_3^- promotes the decomposition of OTF^-, contributing to the transformation of $Zn_5(OH)_8(NO_3)_2{\cdot}2H_2O$ layer into an electrically insulating but ionically conductive SEI. The SEI features ZnF_2-$Zn_5(CO_3)_2(OH)_6$ SEI inner part coated by the organic outer part. The ZnF_2-$Zn_5(CO_3)_2(OH)_6$ inner part removes strongly solvated H_2O around Zn^{2+} before reaching Zn surface, while the organic dominated outer part protects the inner part from significant volume change induced crack during Zn plating/stripping. The fluorinated SEI protected Zn anodes enabled a Zn anode to achieve a reversible and dendrite-free Zn plating/stripping CE of 99.8%, and $Zn||MnO_2$ cells with a low Zn-to-MnO_2 capacity ratio of 2.0 to achieved a high energy density of 168 Wh kg^{-1} (based on cathode and anode) and remained 96.5% of initial capacity after 700 cycles at 10 C.

Keywords: aqueous zinc batteries • insulating passivation layer • convertion • reversibility

[1] a) D. Kundu, S. Hosseini Vajargah, L. Wan, B. Adams, D. Prendergast, L. F. Nazar, *Energy Environ. Sci.* **2018**, *11*, 881-892; b) C. Zhang, W. Ma, C. Han, L.-W. Luo, A. Daniyar, S. Xiang, X. Wu, X. Ji, J. Jia-Xing, *Energy Environ. Sci.* **2021**, *14*, 462-472; c) K. Wu, J. Huang, J. Yi, X. Liu, Y. Liu, Y. Wang, J. Zhang, Y. Xia, *Adv. Energy Mater.* **2020**, *10*, 1903977; d) G. Li, W. Chen, H. Zhang, Y. Gong, F. Shi, J. Wang, R. Zhang, G. Chen, Y. Jin, T. Wu, Z. Tang, Y. Cui, *Adv. Energy Mater.* **2020**, *10*, 1902085.

[2] a) F. Wan, Y. Zhang, L. Zhang, D. Liu, C. Wang, L. Song, Z. Niu, J. Chen, *Angew. Chem. Int. Ed.* **2019**, *58*, 7062-7067; b) Y. Li, B. Liu, J. Ding, X. Han, Y. Deng, T. Wu, K. Amine, W. Hu, C. Zhong, J. Lu, *Batteries & Supercaps* **2020**, *3*, 1-3; c) B. Tang, L. Shan, S. Liang, J. Zhou, *Energy Environ. Sci.* **2019**, *12*, 3288-3304.

[3] a) B.-Q. Li, C.-X. Zhao, S. Chen, J.-N. Liu, X. Chen, L. Song, Q. Zhang, *Adv. Mater.* **2019**, *31*, 1900592; b) N. Wang, X. Dong, B. Wang, Z. Guo, Z. Wang, R. Wang, X. Qiu, Y. Wang, *Angew. Chem. Int. Ed.* **2020**, *59*, 14577-14583.

[4] a) H. Yang, Z. Chang, Y. Qiao, H. Deng, X. Mu, P. He, H. Zhou, *Angew. Chem. Int. Ed.* **2020**, *59*, 9377-9381; b) Y. Yin, S. Wang, Q. Zhang, Y. Song, N. Chang, Y. Pan, H. Zhang, X. Li, *Adv. Mater.* **2020**, *32*, 1906803.

[5] a) L. Kang, M. Cui, F. Jiang, Y. Gao, H. Luo, J. Liu, W. Liang, C. Zhi, *Adv. Energy Mater.* **2018**, *8*, 1801090; b) Y. Jin, K. S. Han, Y. Shao, M. L. Sushko, J. Xiao, H. Pan, J. Liu, *Adv. Funct. Mater.* **2020**, *30*, 2003932.

[6] a) D. Kundu, B. D. Adams, V. Duffort, S. H. Vajargah, L. F. Nazar, *Nat. Energy* **2016**, *1*, 16119; b) Z. Zhao, J. Zhao, Z. Hu, J. Li, J. Li, Y. Zhang, C. Wang, G. Cui, *Energy Environ. Sci.* **2019**, *12*, 1938-1949.

[7] a) H. Qiu, X. Du, J. Zhao, Y. Wang, J. Ju, Z. Chen, Z. Hu, D. Yan, X. Zhou, G. Cui, *Nat. Commun.* **2019**, *10*, 5374; b) A. Naveed, H. Yang, J. Yang, Y. Nuli, J. Wang, *Angew. Chem. Int. Ed.* **2019**, *58*, 2760-2764.

[8] L. Suo, O. Borodin, W. Sun, X. Fan, C. Yang, F. Wang, T. Gao, Z. Ma, M. Schroeder, A. von Cresce, S. M. Russell, M. Armand, A. Angell, K. Xu, C. Wang, *Angew. Chem. Int. Ed.* **2016**, *55*, 7136-7141.

[9] A. Moezzi, M. Cortie, A. M. McDonagh, *Eur. J. Inorg. Chem.* **2013**, *2013*, 1326-1335.

[10] T. Biswick, W. Jones, A. Pacuła, E. Serwicka, J. Podobinski, *J. Solid State Chem.* **2007**, *180*, 1171-1179.

[11] a) D. Hursán, A. A. Samu, L. Janovák, K. Artyushkova, T. Asset, P. Atanassov, C. Janáky, *Joule* **2019**, *3*, 1719-1733; b) J. Liu, M. Jiao, L. Lu, H. M. Barkholtz, Y. Li, Y. Wang, L. Jiang, Z. Wu, D.-j. Liu, L. Zhuang, C. Ma, J. Zeng, B. Zhang, D. Su, P. Song, W. Xing, W. Xu, Y. Wang, Z. Jiang, G. Sun, *Nat. Commun.* **2017**, *8*, 15938.

[12] N. Zhang, F. Cheng, J. Liu, L. Wang, X. Long, X. Liu, F. Li, J. Chen, *Nat. Commun.* **2017**, *8*, 405.

10.1002/anie.202103390

WILEY-VCH

SUPPORTING INFORMATION

Entry for the Table of Contents

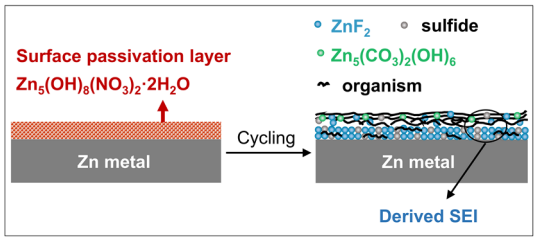

Benefiting from a sacrificail $Zn_5(OH)_8(NO_3)_2{\cdot}2H_2O$ insulating layer, Zn-ion conductive and water-proof fluorine solid electrolyte interphase (SEI) is in situ formed for highly reversible Zn platting/stripping in low-concentration aqueous electrolytes. The in situ formed SEI enables a high Coulombic efficiency of 99.8% for 200 h in Ti||Zn cells, and a high energy density (168 Wh kg^{-1}) with 96.5% retention for 700 cycles in Zn||MnO_2 cells.